JMEPEG (2007) 16:274–283
DOI: 10.1007/s11665-007-9048-9

1059-9495/$19.00

On Practical Forming Limits in Superplastic Forming of Aluminum Sheet

Yingbing Luo, Craig Miller, George Luckey, Peter Friedman and Yinghong Peng

(Submitted December 8, 2006; in revised form January 17, 2007)

In this paper, the superplastic forming (SPF) potential of two fine-grained 5083 aluminum alloys were studied under various stress states with the use of both high temperature tensile testing and pneumatic bulge testing. Experiments with the pneumatic bulge test were performed at temperatures ranging from 475 to 525 °C under three different strain paths ranging from equi-biaxial to approaching plane strain. The effects of temperature on total elongation, *m*-value, final thickness distribution, dome height, and cavitation were investigated for the case of uniaxial and equi-biaxial stretching. Increased temperature in bulge forming was found to improve the thickness distribution in the formed parts, but did not have a significant effect on dome height. The shape of the forming limit diagram (FLD) was found to be significantly different than that of FLDs commonly used in room temperature stamping. Results indicate that determination of forming limits in SPF cannot be represented with a simple FLD and additional metrics such as external thinning and internal cavitation need to be considered to determine a material's SPF potential.

Keywords AA5083, cavitation, forming limit, superplastic forming

1. Introduction

Superplasticity is a term used to indicate the exceptional ductility that certain metals can exhibit when deformed under proper conditions. The tensile ductility of superplastic metals typically ranges from 200 to 1000% elongation, but ductility of 5000% has been reported (Ref 1). Superplastic forming (SPF) is a manufacturing process use an alloy's superplasticity to form sheet components. Typically, superplastic forming takes place in a simple one-sided, single action tool with gas pressure applied to one side of the sheet blank to force the sheet into the forming cavity.

To verify the feasibility and reduce the cost and time of SPF die design, the finite element method (FEM) has been widely adopted in SPF. However, a standard methodology has not been established for evaluating the superplastic formability of sheet metals in FEM. To date, there has been little published research on the formability of superplastic materials in biaxial stretching. Ding et al. (Ref 2) developed a simplified instability criterion based on the Marciniak and Kuczynski (M-K) model (Ref 3) which assumes the existence of an initial imperfection in the sheet which will develop into a groove, however, no experimental results were used to verify the accuracy of this approach. Recently, Chan et al. (Ref 4) and Vulcan et al. (Ref 5) experimentally determined the forming limit diagram (FLD) of SPF by bulge forming one material at one temperature. They found that the shape of the forming limit curve was significantly different from that of traditional forming limit curves.

This work is primarily concerned with the superplastic forming of specially processed 5083 aluminum alloys for automotive applications. The 5083 aluminum alloy has attracted much research interest as the alloy possesses adequate superplasticity with moderate strength, corrosion resistance and weldability (Ref 6-10). For this alloy, cavitation is a critical factor in SPF, which can lead to sheet failure during forming (Ref 11-13) and affect the subsequent service properties (ambient temperature tensile and fatigue) of superplastically formed parts (Ref 14). Cavitation behavior of superplastic materials has been shown to relate to the size and morphology of grains, distribution of intermetallic particles, strain rate and temperature of deformation, stress states, and strain levels (Ref 15-17). In particular for AA5083, Verma et al. (Ref 6) have examined the effect of process parameters such as initial gas pressurization rate, level of hydrostatic pressure, and lubricants on the thinning characteristics of the sheet. Bae and Ghosh (Ref 18-20) studied the cavity formation, growth, and stress state dependence of AA5083. However, less research work has been carried out on the influence of material and temperature on cavitation under biaxial tension.

Within the published literature, the primary method used to characterize superplastic formability has been the elevated temperature uniaxial tensile test. However, biaxial stretching is the dominant stress state in the superplastic sheet blow forming process; therefore, it is more appropriate to study formability and cavitation behavior under biaxial tension. In this paper, experiments were conducted on two superplastic fine-grain 5083 aluminum sheet alloys using both the uniaxial tensile test and biaxial tension pneumatic bulge test at 475, 500, and 525 °C. The FLD was determined from specimens that were

This article was presented at Materials Science & Technology 2006, Innovations in Metal Forming symposium held in Cincinnati, OH, October 15-19, 2006.

Yingbing Luo and **Yinghong Peng,** School of Mechanical Engineering, Shanghai Jiao Tong University, Shanghai 200030, China; **Yingbing Luo, Craig Miller, George Luckey,** and **Peter Friedman,** Ford Research and Innovation Center, 2101 Village Rd, Dearborn, MI 48124, USA. Contact e-mail: yluo8@ford.com.

formed by a pneumatic bulge test with tool ratios of 1:1, 1:0.7, and 1:0.4. The shape of the forming limit curves was found to be different from that of traditional room temperature forming limit curves. In order to determine the influence of temperature and material on cavitation, samples from the formed parts were studied using optimal microscopy. This work demonstrates the complexity of establishing the superplastic forming potential of alloys as a function of temperature and strain rate while considering important elements such as excessive thinning and internal damage (cavitation).

2. Experiment

2.1 Material for study

AA5083 has become the alloy of choice for automotive superplastic forming applications because of its moderate strength, good corrosion resistance, relatively low cost, and ease of processing to achieve a fine grain structure. It has been reported that commercial grades of the specially processed AA5083 alloy can exhibit tensile elongations of over 300% with tensile elongations exceeding 500% in certain grades of the alloy containing lower levels of Fe and Si (Ref 21, 22). To study the influence of materials on forming limits, two commercial superplastic AA5083 alloy sheets provided by different companies were investigated. The chemical composition and initial thickness of the alloys are shown in Table 1. The difference in iron content (Fe) between these two materials should be noted, as increased iron levels are known to reduce formability (Ref 23). The iron combines with other alloying elements to form second-phase particles that act as void-nucleation sites during deformation.

2.2 Experimental Procedure

2.2.1 Tensile Test. The superplastic tension tests on the AA5083 alloy were conducted using an MTS Sintech Machine (MTS Systems Corporation, Eden Prairie, MN) equipped with a three-zone split furnace that maintains the specimen at superplastic temperatures. The load frame was equipped with an 8.9 KN load cell and a computer-controlled data acquisition system. The test procedure began by loading the tensile sample in the Inconel grips which were fastened with faceplates that clamp the grip ends of the specimen. All fasteners used in the Inconel grips were coated with a copper lubricant to allow easy removal after exposure to the elevated temperatures. Once the samples were mounted on the grips, the setup was then fastened to the pull rods of the MTS load frame.

Before the start of the test, the specimens were subject to a 90 min preheat cycle in order achieve a stable target temperature. The average grain size of tensile samples with a 90 min heat-up cycle and sheet formed in an SPF operation with a 2 min heat-up cycle were measured (using the mean linear intercept method) to be 6.6 and 7.8 μm, respectively. It will be demonstrated that the flow stress predicted using coefficients derived from high temperature tensile tests should be adjusted to account for the difference in the average initial grain size of material in a tensile test and an automotive superplastic forming operation.

An initial crosshead velocity was applied based on a target value of initial strain rate. When the specimen elongation reached 5%, the velocity of the crosshead changed based on a second value of target strain rate. This type of a test is called a 'jump test' and can be used to measure a material's strain rate sensitivity (see Section 3.1).

The initial strain rates for the tests performed in this work ranged from 10^{-4} to 2×10^{-2}/s, and are representative of the range of strain rates experienced in the superplastic forming of automotive components. The tests were all 'jump tests' with the exception of two, one with an initial strain rate of 10^{-3}/s and the other at 10^{-2}/s. The test matrix and corresponding crosshead speeds (CHS) are shown in Tables 2 and 3, respectively.

2.2.2 Bulge Forming. The blanks were coated on both sides with a new proprietary Ford Motor Company SPF lubricant that contains boron nitride before forming. The lubricant was received in a water-based suspension to permit spray-on application. The lubricant was allowed to air dry leaving only the solid components of the lubricant on the blank surface. This solid lubricant is capable of withstanding the temperature range (450-550 °C) employed in aluminum superplastic forming and is effective at preventing the sheet from sticking to the die and thus assists in the forming of the sheet and acts as a parting agent during part extraction.

The bulge forming die, shown in Fig. 1, was equipped with insulation and fixed within an 800 Ton SPF press. Forming temperature was maintained in the tool by cartridge heaters embedded in the press platens. Gas pressure was controlled by pneumatically actuated proportional valves, which were dynamically adjusted by the control system. Experiments were carried out in three strain paths at three temperatures for both alloys as shown in Table 4. The tool was equipped with three

Table 1 Chemical composition (in wt.%) and initial thickness of two different AA5083 alloys

Material	Thickness, mm	Mg	Mn	Fe	Si	Cr	Cu	Ti	Al
Alloy A	1.5	4.65	0.68	0.03	0.02	0.11	0.00	0.01	Rest
Alloy B	1.6	4.8	0.53	0.23	0.08	0.08	0.07	0.03	Rest

Table 2 Matrix of superplastic tensile tests

Spec. no.	Orientation	Temperature, °C	Initial strain rate #1, 1/s	Initial strain rate #2, 1/s
A	L	525	1.0E−04	2.0E−04
B	L	525	1.0E−03	2.0E−03
C	L	525	1.0E−02	2.0E−02
D	L	475	1.0E−04	2.0E−04
E	L	475	1.0E−03	2.0E−03
F	L	475	1.0E−02	2.0E−02

Table 3 Initial strain rate and corresponding crosshead speeds used in tensile test

Initial strain rate #1, 1/s	Initial strain rate #2, 1/s	CHS #1, mm/s	CHS #2, mm/s
1.0E−04	2.0E−04	0.00222	0.00466
1.0E−03	2.0E−03	0.02220	0.04662
1.0E−02	2.0E−02	0.22200	0.46220

rings that created three forming orifices: 200 mm circle, 200 mm × 140 mm oval and 200 mm × 80 mm oval (Fig. 2). This equates to major vs. minor ratios of 1:1, 1:0.7, and 1:0.4, respectively. All of the rings were milled to have a 20 mm entry radius to prevent the failure of the sheet at the die entry. Tests were conducted at 475, 500, and 525 °C to study the stress state dependence of SPF formability and cavitation as a function of temperature. Gas pressure was applied based on initial blank thickness, temperature, and tool ratios with a target forming strain rate of 5×10^{-3}/s. All test samples were formed until failure.

A square grid pattern with spacing of 2.54 mm was electrochemically etched onto the surface of the 300×300 mm^2 test samples prior to forming. Samples were pre-heated for 3 min to achieve the target temperature before the press was closed and the blank sealed between the lower and upper die halves. Gas pressure was applied on one side of the sheet forcing the sample to bulge until it failed. In total, 61 parts were formed in the present work with several specimens duplicated. Typical specimens bulged until fracture using the tool ratios of 1:1, 1:0.7, and 1:0.4 are shown in Fig. 3. All bulge test domes failed by splitting near the pole of the dome.

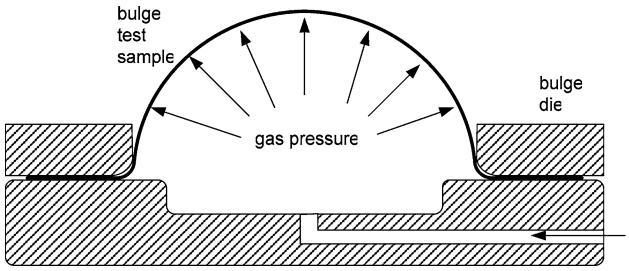

Fig. 1 Schematic of bulge testing apparatus

Table 4 Experimental factors used in bulge test forming trials

Tool ratio	Material	Temperature, °C
0.7, 0.4	Alloy A, Alloy B	475, 500, 525

3. Experimental Results

3.1 Tensile Test

Load vs. extension data were converted to true strain-true stress based on the assumption of uniform straining within the gauge section. Although the diffuse neck that occurs during superplastic tensile testing violates this assumption, the calculated strain is used to compare the flow behavior of the two alloys. Figure 4(a) shows the flow stress vs. strain for samples deformed at three different initial strain rates at 525 °C. Flow stresses for samples deformed under the same three conditions, but at a lower temperature of 475 °C are shown in Fig. 4(b). All of the curves show a rapid increase in flow stress at approximately 5% strain, which correlates with the jump in strain rate used to measure the strain-rate sensitivity of the material. In the high strain-rate test, there is a slight drop in flow stress immediately before the strain rate jump. This is due to an inertial effect in the load frame as it shifts into the higher speed. This effect has been ignored in the calculation of *m*-value by using the flow stress value just prior to the sudden drop in stress. For both materials, the flow stress appears to be highly correlated with strain rate with the faster rate showing significantly higher flow stress (Ref 24).

Total elongation is often used as a measure of a material's formability and is typically shown as a function of strain rate and temperature. The total elongations for test alloys at 525 and 475 °C are plotted as a function of log (initial) strain rate and shown in Fig. 5(a) and (b), respectively. Elongation appears to

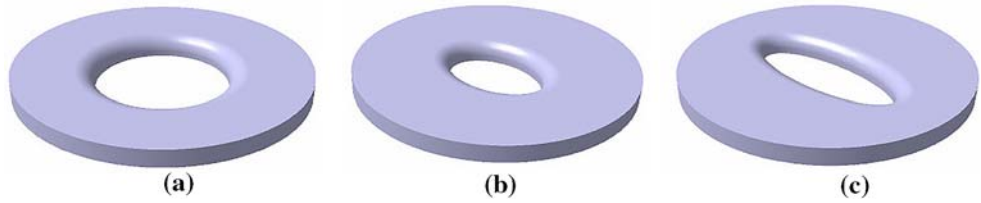

Fig. 2 Die inserts for bulge test apparatus with aspect ratios of (a) 1:1, (b) 1:0.7, and (c) 1:0.4

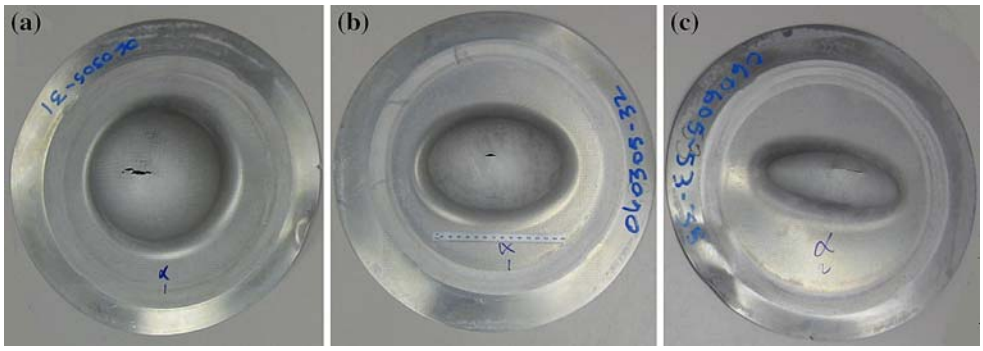

Fig. 3 Panels formed with aspect ratios of (a) 1:1, (b) 1:0.7, and (c) 1:0.4

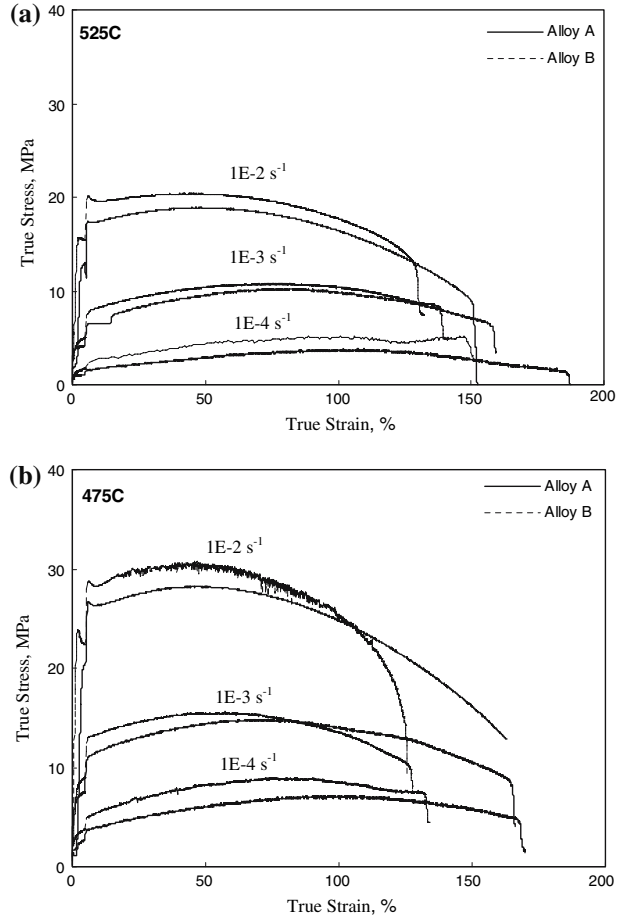

Fig. 4 True stress-true stain as determined by tensile test for alloys A and B at (a) 525 °C and (b) 475 °C

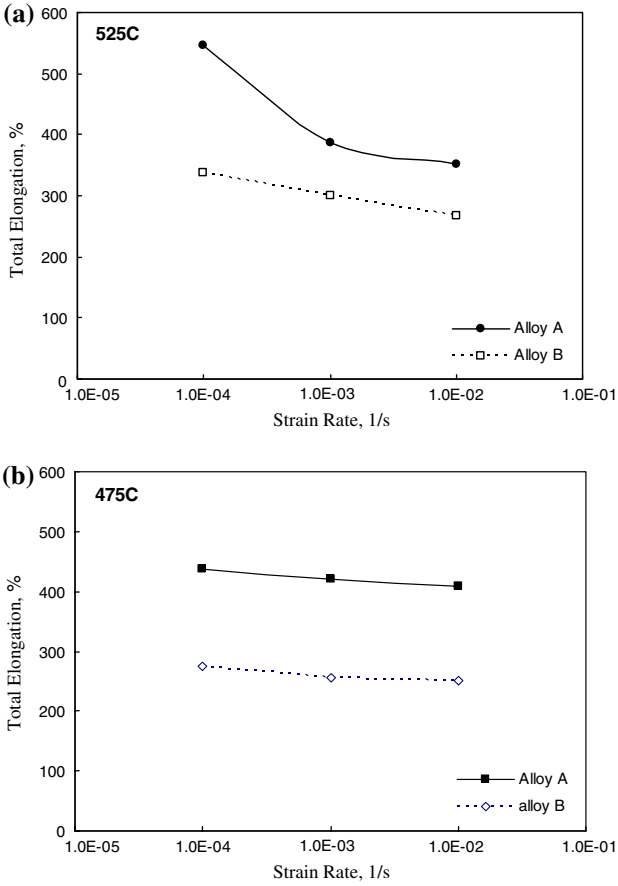

Fig. 5 Total elongation plotted as a function of log strain rate for samples tested at (a) 525 °C and (b) 475 °C

be correlated with strain rate with the samples deformed at the slower strain rates showing larger elongations.

The strain-rate sensitivities (*m*-value) are plotted in Fig. 6(a) and (b) as a function of log initial strain rate for the two alloys at 525 and 475 °C, respectively. The data demonstrate the bell shape curvature that is typical of superplastic materials. The effect of temperature on *m*-value can be seen by comparing Fig. 6(a) and 6(b), where the strain-rate sensitivities of the test alloys at 475 °C are significantly lower than those at 525 °C.

While the data presented above represent the strain-rate sensitivities at 5% elongation for all of the samples, it is interesting to look at the strain-rate sensitivity of the material as a function of strain. To accomplish this, the flow stress data for each sample at 10% strain increments were extracted from the flow data. Flow stress from samples deformed at the slowest rate and middle rate were used as well as data from the medium rate and fastest rate. The strain rate sensitivity was calculated according to Eq (1):

$$m = \left(\frac{\log(\sigma_2/\sigma_1)}{\log(\dot{\varepsilon}_2/\dot{\varepsilon}_1)}\right) \qquad \text{(Eq 1)}$$

where σ_1 and σ_2 are the flow stresses $\dot{\varepsilon}_1$ and $\dot{\varepsilon}_2$ are the corresponding instantaneous strain rates for the two different tests at equal increments of strain, respectively.

The calculated *m*-value was assumed to correspond to the average of the two strain rates that were compared. A particular strain rate was compared to all other strain rate values that were greater. The *m*-value then was plotted as a function of log initial strain rate. A linear equation was fit to the data and was used to calculate an *m*-value for a particular initial strain rate. This linear equation was then used to calculate an *m*-value for a specific initial strain rate.

As shown in Fig. 7, the two alloys appear to behave similarly with the *m*-value decreasing with strain. The decrease is believed to be a result of a combination of grain growth and damage accumulation in the form of cavity nucleation and growth. The data taken from both alloys deformed at 10^{-4} and 10^{-3}/s strain rates show significantly higher *m*-values than data taken from samples deformed at 10^{-3} and 10^{-2}/s. This is consistent with the data shown in Fig. 6, where the *m*-value at the lower strain rates was higher than those at the faster strain rates.

3.2 Forming Limit Diagram

The limits of formability for sheet metals are often described in terms of the principal strains (major and minor strains), which are calculated by measuring grid patterns etched on the sheet prior to forming, by constructing an FLD (Ref 25). An FLD divides the region of strain field that is safe for a specific forming operation from the one that can lead to fracture. As in FEM, most formability data on conventional automotive sheet metals have been built in terms of FLD, therefore, efforts have been made to construct an FLD for the SPF process.

In the present work, square grid patterns were printed on all the samples by a chemical etching method. As the sheet

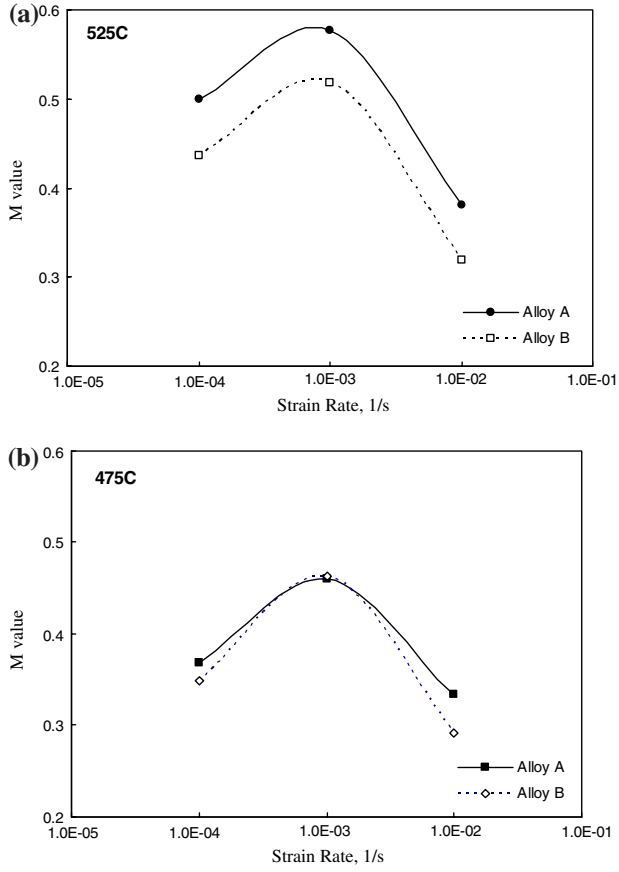

Fig. 6 Strain-rate sensitivity (*m*-value) plotted as a function of log strain rate for samples tested at (a) 525 °C and (b) 475 °C

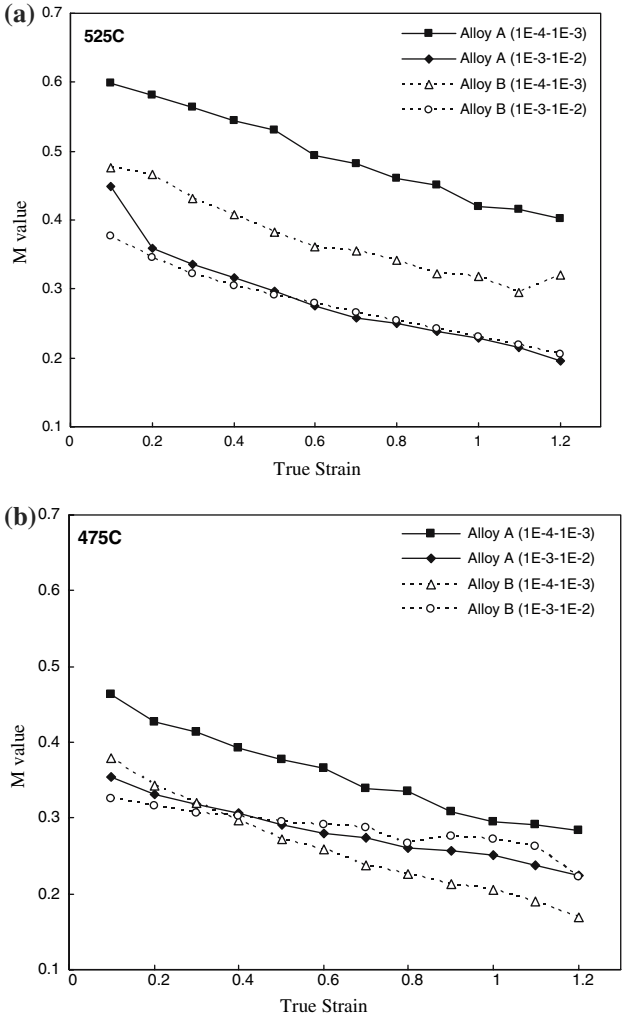

Fig. 7 Strain-rate sensitivity (*m*-value) plotted as a function of true strain for samples tested at (a) 525 °C and (b) 475 °C

samples were subjected to different states of stress, the square deformed to different shapes. The major length and minor length of the grids were measured using a traveling microscope to calculate major strain (ε_1) and minor strain (ε_2). For each part, major strain (ε_1) and minor strain (ε_2) were measured on three grids adjacent to (limit strain) and one grid away from (safe strain) fracture. An example of an FLD is shown in Fig. 8, where the major strain vs. minor strain is plotted for different tool ratios. There appears to be significant scatter in the data for all three aspect ratios.

According to the method described above, FLDs of alloys A and B at three different forming temperatures (475-525 °C) were developed and plotted in Fig. 9. The limit strains determined experimentally were very sensitive to tool ratio and increase as the strain ratio decreases. The trend of the FLD in SPF is different from that of conventional forming at room temperature. Similar results have been reported by Chan et al. (Ref 9) and Vulcan et al. (Ref 10) for AA5083 alloy at 550 °C.

As shown in Fig. 9 the limit strains decrease dramatically as the temperature increases from 475 to 525 °C, which is different from the result of uniaxial tensile test, which typically show improved formability with increasing temperature (Ref 26). It is shown in Fig. 9(a) that alloy A is sensitive to tool ratio at all temperatures; however, for alloy B (Fig. 9b), the limit strain becomes insensitive to tool ratio.

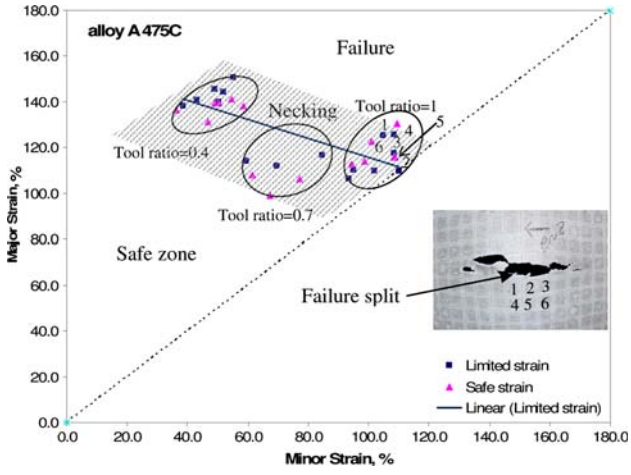

Fig. 8 A map of major and minor strains measured from pre-etched grids around a crack (see inserted photo showing an example of how the FLD was constructed)

3.3 Dome Height

The peak height of the bulge samples was measured on FLD samples of both alloys at all three temperatures and plotted as a function of tool aspect ratio in Fig. 10. Dome height appears to be sensitive to tool ratio and increases dramatically with increasing tool ratio for both alloys. At 475 °C, the dome

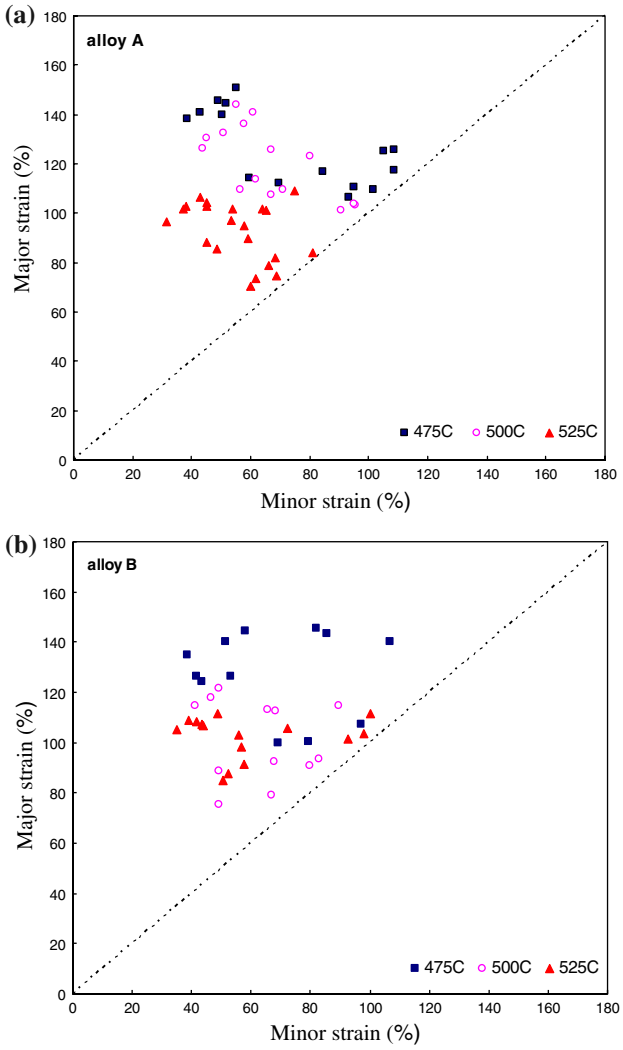

Fig. 9 Forming limit diagram at different temperatures for (a) alloy A and (b) alloy B

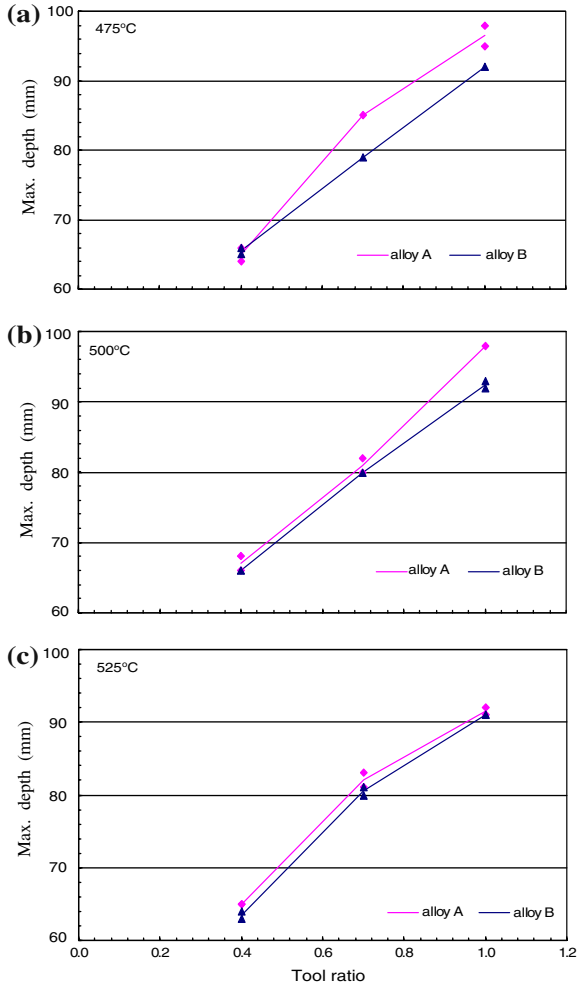

Fig. 10 Dome height plotted as a function of tool ratio for tests performed at (a) 475 °C, (b) 500 °C, and (c) 525 °C

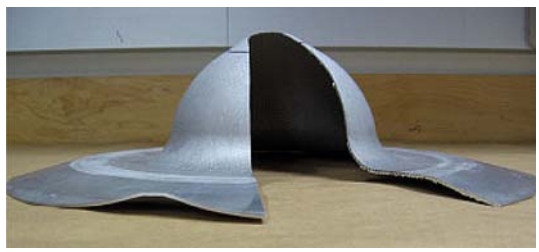

Fig. 11 Photograph of a cut part for measurement of thickness distribution

height of alloy A is greater than that of alloy B for aspect ratios of 1.0 and 0.7. The alloys both show a similarly low dome height for aspect ratio of 0.4. Similar results are shown in Fig. 10(b) and (c) for temperatures of 500 and 525 °C, respectively. The dome height of alloy A appears to be higher than that of alloy B for most of the conditions. Although the difference is relatively small, it is consistent at all conditions, which indicates superior formability in alloy A.

3.4 Thickness Distribution

In order to investigate the thickness distribution of deformed parts, specimens were cut along the 0 and 45° section, as shown in Fig. 11. A thickness gauge was used to measure the thickness along the cross section and thickness reduction was calculated and plotted as a function of location along the cross section as shown in Fig. 12. The thickness reduction in both alloys appears to decrease with increasing temperature. For alloy A, the maximum thickness reduction at 475 and 525 °C are 76 and 65%, respectively. As shown in Fig. 12(b), the influence of temperature on final thickness reduction for alloy B is consistent with that of alloy A. This relationship of temperature and thickness reduction can explain the measured effect temperature had on the FLD and dome height. While increases in temperature will cause smaller limit major/minor strains at fracture, it does not have a significant effect on dome height. The increased temperature results in more uniform flow and superior thickness distribution, which is consistent with the tensile test data that showed higher m-values with increasing temperature.

3.5 Cavitation

To measure the extent of cavitation in the deformed regions, samples were extracted from the formed parts (Fig. 13) and

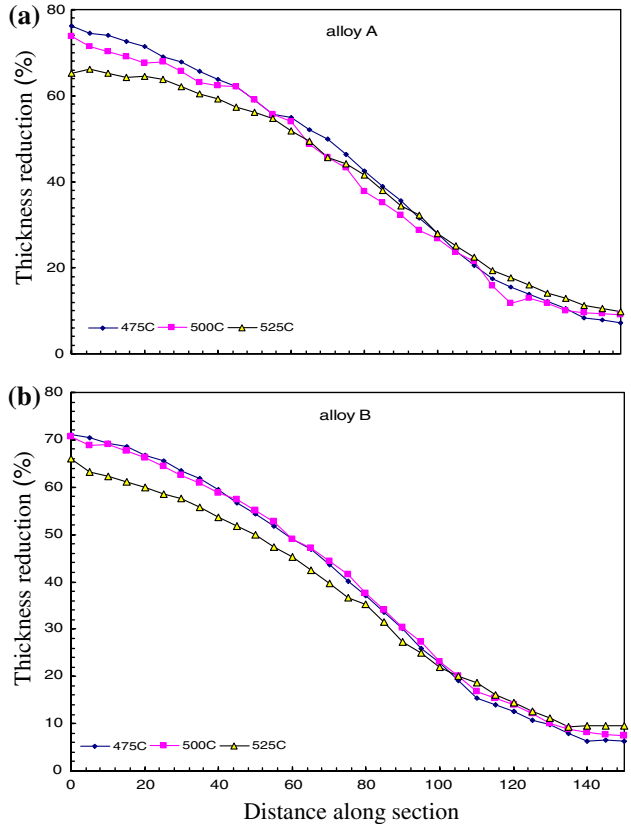

Fig. 12 Thickness reduction plotted as a function of distance along section, starting from the center of sample

Fig. 13 Schematic of the sample from bulge specimen used to study the cavitation behavior

investigated with optical microscopy. Metallographic samples were prepared by mechanically polishing and etching with Graf Sergeant reagent (15.5 mL HNO_3, 0.5 mL HF, 3 g Cr_2O_3, and 84 mL water). All of the metallographic sections in this work are shown in the L-S orientation (rolling direction parallel to the horizontal, thickness parallel to the vertical).

Micrographs of samples of alloy B deformed to various strain levels at 500 °C are shown in Fig. 14. Cavities appear randomly distributed and cavity size varies over a wide range. With increasing strain, the population (number density) and average size of cavities appear to increase. The population increase is believed to be directly related to the emergence of new small size cavities. At a strain of 1.19 (failure), coalesced cavities are found at several locations.

The effect of temperature on cavitation is presented in Fig. 15, from samples tested to a strain of 0.64 for the three test temperatures. At the lowest test temperature of 475 °C, the size of cavities is generally smaller. At 525 °C, the number density of cavities is larger than that of the other temperatures, and cavity shape is irregular.

The fraction of cavities, which can be approximated as the area fraction of cavities, is the sum of the products of the population and size of individual cavities. Two-dimensional measurements of cavities on the cutting planes were conducted via computer imaging using the method discussed in Ref 24. Cavitation area fraction plotted as a function of strain and thickness reduction for biaxial tension at different temperatures is shown in Fig. 16 and 17, respectively. From Fig. 16(a) and (b), it can be found that for the same threshold value of cavitation area fraction, similar thickness reduction can be achieved in both alloys at all three temperatures (e.g., for a cavitation area fraction (V) of 2% the thickness reduction is approximately 55-60% regardless of temperature or alloy). Cavitation area fraction as a function of strain is plotted in a semi-logarithmic scale in Fig. 17(a) and (b) for the three different test temperatures. The area fraction of cavities increases nearly exponentially with strain (except for alloy B at 525 °C which had excessive cavitation along the entire cross section), which is in agreement with the data of other superplastic materials including aluminum alloys (Ref 18-20). This suggests that void growth in this material deformed under these conditions is essentially controlled by plasticity (Ref 15). The slope of these plots, $\eta = d \ln V/d\varepsilon$ (termed the cavity growth rate factor), is indicated in Fig. 17 next to each curve in the strain range showing a linear relationship. This value of η appears to be higher with increased temperature for both alloys A and B, showing that higher temperature will accelerate cavitation growth and nucleation.

4. Discussion

A major issue in quantifying the SPF potential of an alloy is the role of cavitation in failure. Aluminum alloys, especially Al-Mg alloys, under superplastic conditions typically fail by cavitation. However, degradation of the materials room temperature properties starts well before fracture. Hence, quantifying the cavitation behavior of an alloy is of critical importance. Cavity growth in superplastic deformation is typically controlled by plastic flow; therefore, it is possible that samples deformed at slower strain rates and higher temperatures can withstand a higher cavitation volume because of the lower forces on the grain boundaries. This can explain the higher total elongations found at the slowest strain rates during uniaxial tensile testing as compared to the middle rate where m-value is greatest.

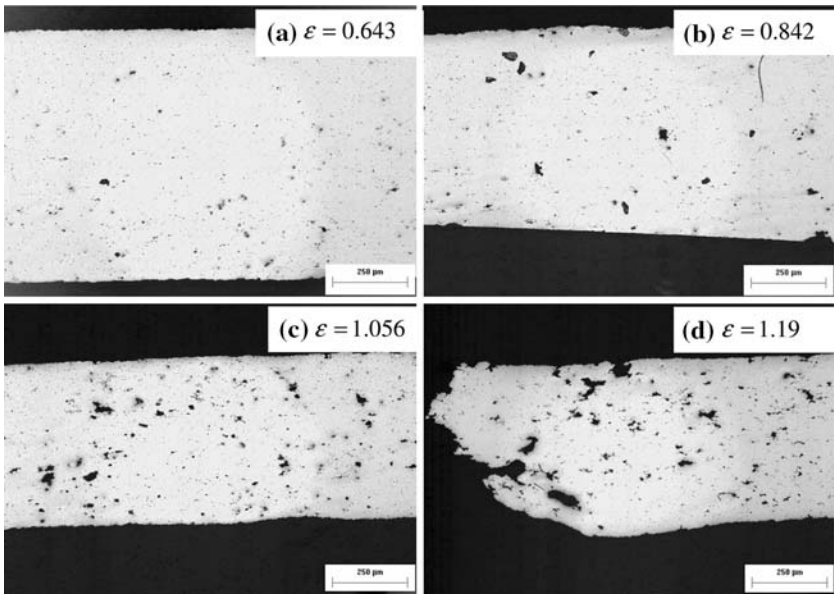

Fig. 14 Micrographs showing: (a)-(d) progress of cavitation of alloy B with strain at 500 °C

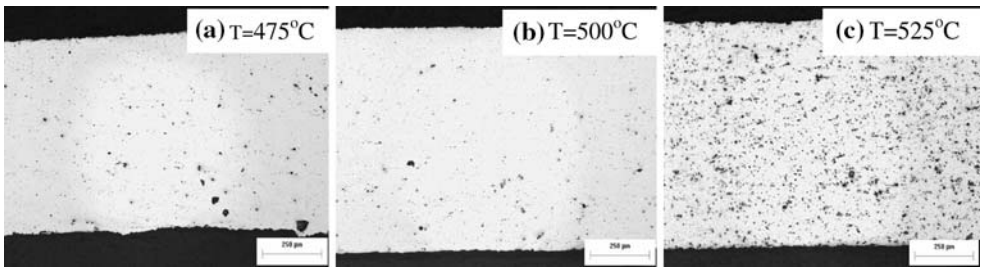

Fig. 15 Micrographs showing: (a)-(c) effect of temperature on cavitation of alloy B for ε = 0.64 and temperatures of 475, 500, and 525 °C, respectively

Results of the bulge testing for all forming conditions show significant scatter in terms of failure strain. This scatter is due to several factors but can best be explained by the way in which these materials accumulate damage and eventually fail. As noted above, fracture in these alloys is typically controlled by the initiation, growth, and eventual coalescence of cavities (or voids). This is a complicated, dynamic process in which a wide variety of cavity formations can be created. The low-flow stresses in SPF make it possible for the material to continue to form even though the material contains significant cavitation. Strain measurements taken from grid analysis do not accurately quantify the true bulk damage in the material and therefore result in significant scatter. Furthermore, the FLD is a misleading indicator of formability since cavitation can cause a significant reduction in the post-form (or in-service) properties of the material well before fracture. The true failure of the material should be considered to be when the material has attained a certain level of cavitation rather than when the material actually splits.

Dome height appears to be sensitive to tool ratio and increases dramatically with increasing tool ratio for both alloys. The dome height of alloy A was found to be slightly higher than that of alloy B for all test conditions. Comparison of thickness reduction for different temperatures shows that there is more uniform flow at higher temperatures, which is consistent with the elevated temperature tensile test data showing higher strain rate sensitivity with increasing temperature.

Based on this work, it appears unlikely that a single test method can provide useful, practical forming limits. Instead an approach utilizing the two test methods of elevated temperature tensile test and biaxial stretch forming can likely provide sufficient data that is both repeatable and physically meaningful. The tensile elongation of the elevated temperature tensile test offers little insight into the materials formability during biaxial stretch forming. However, it is essential for generating data to develop constitutive equations needed for FEA simulation of the forming process. Furthermore, the tensile test provides an accurate method of measuring strain-rate sensitivity, which is a good and intuitive metric for assessing a materials ability to resist necking. This is a critical parameter for things such as establishing the minimum radius size in which a material can be formed over within a die cavity.

The biaxial dome test provides stretch forming data from a die cavity that is reasonably indicative of industrial gas forming operations. The output of the test, dome height and thickness reduction, provide useful and quantifiable data that may be applicable to establish suitable criterion for determining practical forming limits when coupled with proper consideration of the role of cavitation.

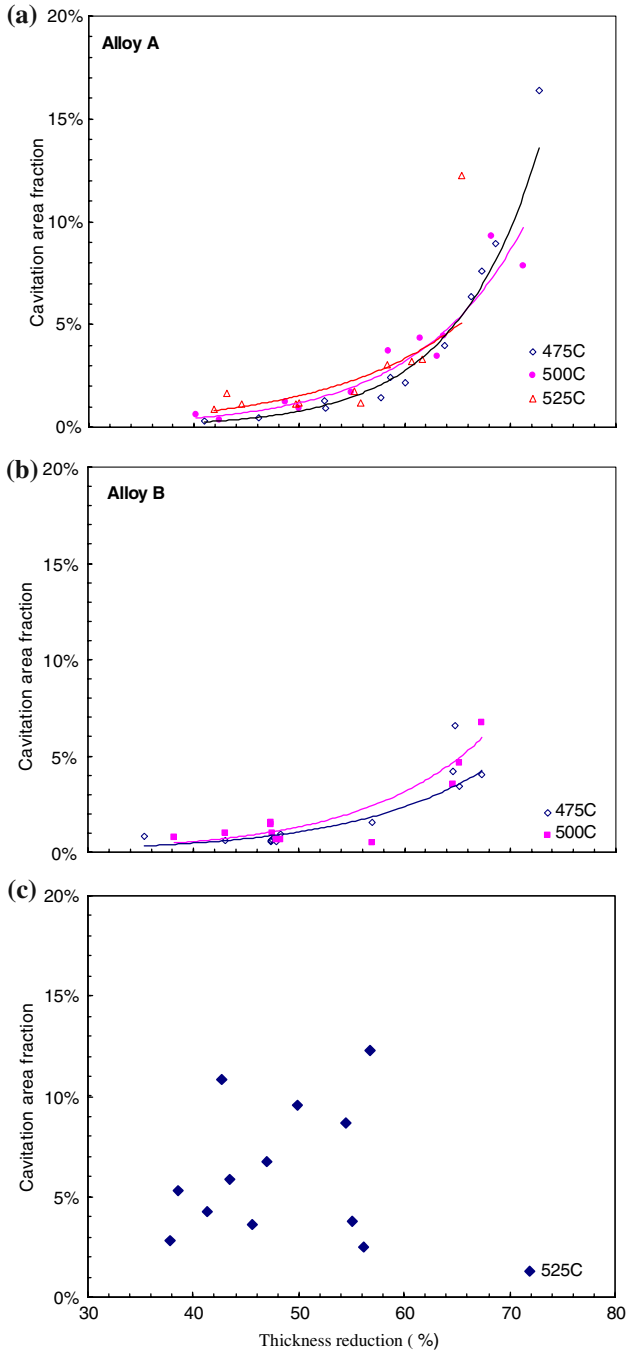

Fig. 16 Cavitation area fraction plotted as a function of thickness reduction for biaxial tension at different temperatures

5. Summary and Conclusions

This research focuses on the failure modes for superplastic materials and considers the metrics necessary to establish practical superplastic forming limits for aluminum sheet. Experiments were performed at temperatures ranging from 475 to 525 °C with tensile test and under three different strain paths ranging from equi-biaxial to approaching plane strain using a pneumatic bulge test. The effects of temperature on final thickness distribution, dome height, and cavitation were investigated for the case of equi-biaxial stretching. Although

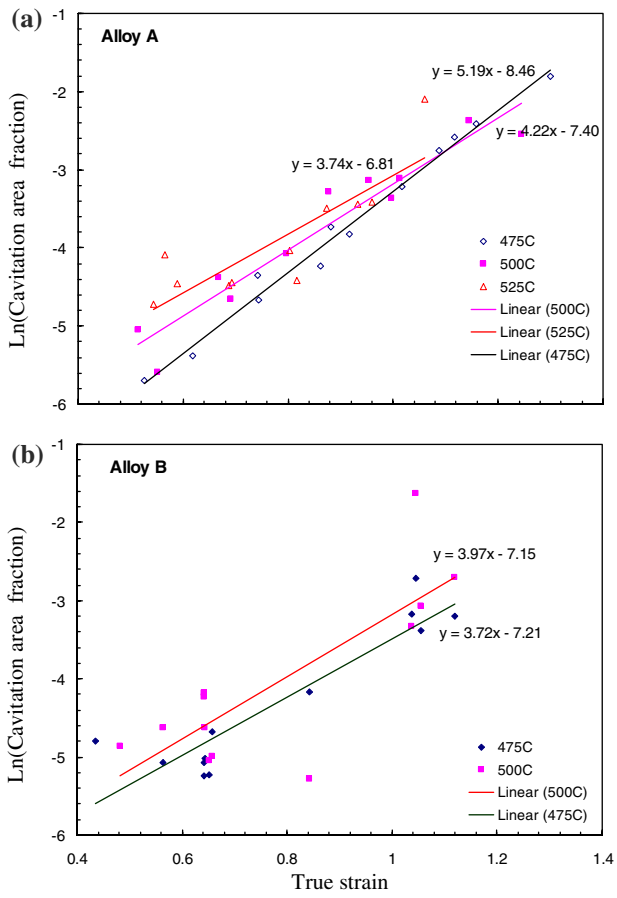

Fig. 17 Cavitation area fraction plotted as a function of true strain for biaxial tension at different temperatures

results indicate that both the tensile and bulge tests have significant limitations in terms of accurately quantifying a materials practical forming limit in SPF, when used in conjunction, they offer valuable insight into a material's superplastic formability.

References

1. C.H. Hamilton, A.K. Ghosh, Superplastic Sheet Forming, *Metals Handbook*, ASM, 1988, p 852–869
2. X.D. Ding, H.M. Zbib, C.H. Hamilton, and A.E. Bayoumi, On the Stability of Biaxial Stretching with Application to the Optimization of Superplastic Blow-Forming, *J. Eng. Mater. Technol.*, 1997, **119**, p 26–31
3. Z. Marciniak and K. Kucznski, Limit Strains in the Processes of Stretch-Forming Sheet Metal, *Intl. J. Mech. Sci.*, 1967, **9**, p 609–620
4. K.C. Chan and K.K. Chow, Analysis of Hot Limit Strains of a Superplastic 5083 Aluminum Alloy Under Biaxial Tension, *Intl. J. Mech. Sci.*, 2002, **44**, p 1467–1478
5. M. Vulcan, K. Siegert, Forming Limited Diagram of a Superplastic Formable AA5083 Aluminum Alloy. Advances in Superplasticity and Superplastic Forming, *Proc. TMS Conf.*, E.M. Taleff, P.A. Friedman, P.E. Krajewski, R.S. Mishra, and J.G. Schroth, Eds., 2004, p 351–360
6. R. Verma, P.A. Friedman, A.K. Ghosh, S. Kim, and C. Kim, Characterization of Superplastic Deformation Behavior of a Fine Grain 5083 Al Alloy Sheet, *Metal. Trans. Mater. Ser. A*, 1996, **27**, p 1889–1898
7. H. Iwasaki, H. Hosokawa, T. Mori, T. Tagata, and K. Higashi, Quantitative Assessment of Superplastic Deformation Behavior in a Commercial 5083 Alloy, *Mater. Sci. Eng. A*, 1998, **252**, p 199–202

8. K. Kanna, C.H. Johnson, and C.H. Hamilton, A Study of Superplasticity in a Modified 5083 AL-Mg-Mn alloy, *Metal. Trans. Mater. Ser. A*, 1998, **29**, p 1211–1120
9. S.N. Patankar and T.M. Jen, Inhomogeneities in Initial Cavity Distribution in a Superplastic Al5083 Alloy, *Scripta Mater.*, 1998, **38**(8), p 1255–1261
10. P.A. Friedman and A.K. Ghosh, Microstructural Evolution and Superplastic Deformation Behaviour of Fine Grain 5083Al, *Metal. Trans. Mater. Ser. A*, 1996, **27**, p 3827–3839
11. X.G. Jiang, J.C. Earthman, and F.A. Mohamed, Cavitation and Cavity-induced Fracture During Superplastic Deformation, *J. Mater. Sci.*, 1994, **29**, p 5499–5506
12. E.M. Taleff, D.R. Lesuer, and J. Wadsworth, Enhanced Ductility in Coarse-grained Al-Mg Alloys, *Metal. Mater. Trans. A*, 1996, **27A**, p 343–352
13. K.C. Chan and G.Q. Tong, The Cavitation Behavior of a High-strain-rate Superplastic Al6061/20SiCw Composite Under Uniaxial and Equibiaxial Tension, *Scripta Mater.*, 1998, **38**, p 1705–1710
14. C.C. Bampton, The Effect of Superplastic Deformation on Subsequent Service Properties of Fine Grained 7475Al. *J. Eng. Mater. Technol*., 1983, **105**, p 55–60
15. J. Pilling and N. Ridley, Effect of Hydrostatic Pressure on Cavitation in Superplastic Aluminium Alloys, *Acta Mater.*, 1986, **34**, p 669–679
16. K.K. Chow and K.C. Chan, The Cavitation Behavior of a Coarse-grained Al5052 Alloy Under Hot Uniaxial and Equibiaxial Tension, *Mater. Lett.*, 2001, **49**, p 189–196
17. Z.X. Guo and N. Ridley, Modeling of Super Plastic Bulge Forming of Domes, *Mater. Sci. Eng. A*, 1989, **121**, p 97–104
18. D.H. Bae and A.K. Ghosh, Cavity Formation and Early Growth in a Superplastic Al-Mg Alloy, *Acta Mater.*, 2002, **50**, p 511–523
19. D.H. Bae and A.K. Ghosh, Cavity Growth in a Superplastic Al-Mg Alloy: I. Experimental Study, *Acta Mater.*, 2002, **50**, p 993–1009
20. D.H. Bae, A.K. Ghosh, and J.R. Bradley, Stress-State Dependence of Cavitation and Flow Behavior in Superplastic Aluminum Alloys, *Metal. Mater. Trans.*, 2003, **34A**, p 2449–2463
21. H. Imamur, and N. Ridley, Superplastic Behaviour in a Commercial 5083 Aluminium Alloy, *Proc. Intl Conf. in Superplasticity of Advanced Materials, ICSAM*'91, Osaka, Japan, S. Hori, M. Tokizane, and N. Furushiro, Eds., 1991, p 453–458
22. J.S. Vetrano, C.A. Lavender, C.H. Hamilton, M.T. Smith, and S.M. Bruemmer, Superplastic Behaviour in a Commercial 5083 Aluminium Alloy, *Scripta Metal. Mater.*, 1994, **30**(3), p 565–570
23. W.B. Lievers, A.K. Pilkey, and D.J. Lioyd, The Influence of Iron Content on the Bendability of AA6111 Sheet, *Mater. Sci. Eng. A*, 2003, **361**, p 312–320
24. P.A. Friedman and W.B. Copple, Superplastic Response in Al-Mg Sheet Alloys, *J. Mater. Eng. Perform.*, 2004, **13**, p 335–347
25. S.P. Keeler, Determination of Forming Limits in Automotive Stampings, *Sheet Mental Industry*, 1965, **42**, p 683–691
26. R.M. Cleveland, A.K. Ghosh, and J.R. Bradley, Comparison of Superplastic Behavior in Two 5083 Aluminum Alloys, *Mater. Sci. Eng. A*, 2003, **351**, p 228–236